

Search for inhomogeneous Meissner screening in Nb induced by low-temperature surface treatments

Ryan M. L. McFadden^{1,2} and Tobias Junginger^{1,2}

¹TRIUMF, 4004 Wesbrook Mall, Vancouver, BC V6T 2A3, Canada

²Department of Physics and Astronomy, University of Victoria, 3800 Finnerty Road, Victoria, BC V8P 5C2, Canada

(*Authors to whom correspondence should be addressed: rmlm@triumf.ca; and junginger@uvic.ca)

(Dated: 26 August 2024)

Empirical surface treatments, such as low-temperature baking (LTB) in a gaseous atmosphere or in vacuum, are important for the surface preparation of Nb superconducting radio frequency (SRF) cavities. These treatments inhomogeneously dope the first ~ 50 nm of Nb's subsurface and are expected to impart depth-dependent characteristics to its Meissner response; however, direct evidence supporting this remains elusive, suggesting the effect is subtle. In this work, we revisit the Meissner profile data for several LTB treatments obtained from low-energy muon spin rotation (LE- μ SR) experiments [A. Romanenko *et al.*, *Appl. Phys. Lett.* **104**, 072601 (2014) and R. M. L. McFadden *et al.*, *Phys. Rev. Appl.* **19**, 044018 (2023)], and search for signatures of inhomogeneous field screening. Using a generalized London expression with a recently proposed empirical model for a depth-dependent magnetic penetration depth $\lambda(z)$, we obtain improved fits to the Meissner data, revealing that the presence of a non-superconducting surface “dead layer” $d \gtrsim 25$ nm is a strong indicator of a reduced supercurrent density at shallow subsurface depths. Our analysis supports the notion that vacuum annealing at 120 °C for 48 h induces a depth-dependent Meissner response, which has consequences for Nb's ability to maintain a magnetic-flux-free state. Evidence of similar behavior from a “nitrogen infusion” treatment is less compelling. Suggestions for further investigation into the matter are provided.

I. INTRODUCTION

Low-temperature baking (LTB) treatments are important for the surface preparation of Nb superconducting radio frequency (SRF) cavities^{1–3} — a class of superconducting resonators⁴ used in particle accelerators. These procedures, performed either in vacuum^{5,6} or in a low-pressure gaseous environment,^{7,8} induce changes to Nb's supercurrent density in its near-surface region through the introduction of intrinsic (e.g., dissolved oxygen from its surface oxide layer⁵) or extrinsic (e.g., infused nitrogen from the treatment atmosphere⁸) shallow impurity profiles. Chiefly, these treatments are known to mitigate the high-field Q slope (HFQS) in SRF cavities,^{9–12} wherein a sudden drop in a cavity's quality factor Q is coincident with a sharp increase in its surface resistance.³ Their mechanism of action is thought to be connected to the nanoscale alternations taking place in Nb's near-surface region (i.e., the topmost ~ 50 nm), where empirical observations^{8,10,12} and model predictions^{13–15} suggest that the treatment-induced defects are *inhomogeneous* with depth. Of particular interest is how this impacts Nb's ability to remain in a flux-free Meissner state,^{16–20} which is essential for SRF cavity operation.³ As several material properties are proportional to impurity concentration (e.g., carrier mean-free-path ℓ ^{21,22}), they too are expected to vary non-uniformly below the surface, which should influence the element's Meissner response,^{12,15,23} however, directly probing their influence remains challenging.

Early measurements on a Nb SRF cavity cutout baked at 120 °C for 48 h (which we refer to henceforth as “120 °C bake”) showed an abrupt discontinuity in its Meissner profile,²⁴ suggesting the presence of a spatially inhomogeneous near-surface supercurrent density. Among the initial efforts to model this behavior (see, e.g., Refs. 25,26), one approach,²⁷ in analogy with superconducting multilayers,^{28–31} approximated the inho-

mogeneous surface region as a superconductor-superconductor (SS) bilayer (i.e., a thin “dirty” layer atop a “clean” substrate), correctly reproducing the treatment's abated near-surface supercurrent density.²⁷ Despite this breakthrough,³² subsequent measurements on a similarly treated Nb sample showed no such feature,³³ with true bilayer samples also producing distinct screening properties.³⁴ These differences were explained in a recent commentary,³⁵ with the discontinuity attributed to an analysis artifact. Interestingly, this work also uncovered a large non-superconducting surface “dead layer” $d \approx 35$ nm.³⁵ While $d \gtrsim 5$ nm for Nb is common,^{24,33,36–38} likely due to the roughness^{39,40} introduced by its surface oxidation,⁴¹ such a large value is suggestive of a surface-localized region with a diminished screening capacity. This finding is consistent with the shallow impurity profiles found in closely related LTB treatments,^{15,42,43} which are predicted to “distort” the Meissner profile close to the surface (see, e.g., Ref. 15). The effect is, however, likely both gradual and subtle,^{15,35} requiring scrupulous inspection.

In this work, we revisit measurements of Nb's Meissner screening profile obtained by low-energy muon spin rotation (LE- μ SR)^{44,45} — a sensitive, non-destructive technique for interrogating subsurface magnetic fields with nanometer depth resolution — for several LTB treatments and search for evidence of spatially inhomogeneous screening. Specifically, we examine results obtained for: a Nb SRF cavity “cold spot” cutout whose surface underwent electro-polishing (EP)⁴⁶ + 120 °C baking⁵ (see Refs. 24,35 and Figure 1); an SRF-grade Nb plate with a surface prepared by buffered chemical polishing (BCP)⁴⁶ + 120 °C baking⁵ (see Ref. 33 and Figures 2 and 4); and another SRF Nb plate with a surface prepared by BCP⁴⁶ + “N₂ infusion”⁸ (see Ref. 33 and Figures 3 and 4). By comparing the form of the each sample's screening profile against a recently proposed phenomenological model,¹² we search for signatures

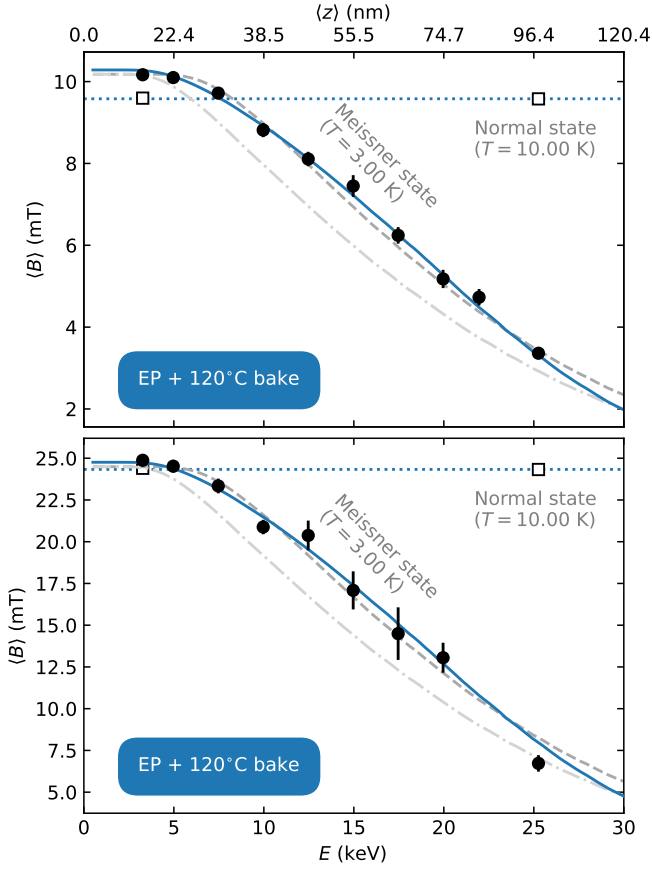


FIG. 1. Meissner screening data (at two different applied fields) in a Nb SRF cavity cutout “cold spot” with an “EP⁴⁶ + 120°C bake⁵” surface treatment, obtained from LE- μ SR experiments originally reported in Ref. 24 (and recently re-analyzed in Ref. 35). Here, the mean magnetic field $\langle B \rangle$ is plotted against the muon μ^+ implantation energy E , with its corresponding mean stopping depth $\langle z \rangle$ indicated on a secondary axis. The solid and dotted colored lines denote simultaneous fits of the normal and Meissner state data to Equations (1), (4) and (5). For comparison, the dashed dark gray line shows the form of $\langle B \rangle(E)$ assuming a single (i.e., depth-independent) magnetic penetration depth λ [Equations (1) to (3)]. The dash-dot light gray line denotes this average screening behavior, but with its non-superconducting “dead layer” d adjusted to match the fit using the generalized London equation, highlighting the differences between the two models.

of inhomogeneous screening.

II. EXPERIMENTAL BACKGROUND & THEORY

In LE- μ SR,^{44,45} positive muons μ^+ (spin $S = 1/2$; gyromagnetic ratio $\gamma/(2\pi) = 135.539 \text{ MHz T}^{-1}$; mean lifetime $\tau = 2.197 \mu\text{s}$) are implanted in a host material at an energy E between 0.5 keV to 30 keV, where they probe subsurface electromagnetic fields at depths up to $\sim 200 \text{ nm}$.⁴⁷ The technique is highly sensitive to spatial gradients in magnetic field, making it well-suited for the study of Meissner profiles.⁴⁵ In the measurement, one observes the μ^+ spin-precession signal (detected via its radioactive decay products), which provides

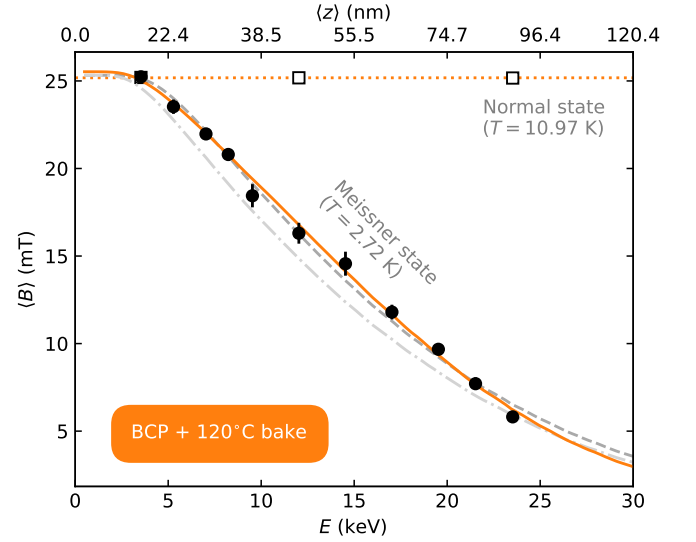


FIG. 2. Meissner screening data in an SRF-grade Nb plate with a “BCP⁴⁶ + 120°C bake⁵” surface treatment, obtained from LE- μ SR experiments originally reported in Ref. 33. Here, the mean magnetic field $\langle B \rangle$ is plotted against the muon μ^+ implantation energy E , with its corresponding mean stopping depth $\langle z \rangle$ indicated on a secondary axis. The solid and dotted colored lines denote simultaneous fits of the normal and Meissner state data to Equations (1), (4) and (5). For comparison, the dashed dark gray line shows the form of $\langle B \rangle(E)$ assuming a single (i.e., depth-independent) magnetic penetration depth λ [Equations (1) to (3)]. The dash-dot light gray line denotes this average screening behavior, but with its non-superconducting “dead layer” d adjusted to match the fit using the generalized London equation, highlighting the differences between the two models.

a measure of the field distribution $p(B)$ sampled by the μ^+ stopping profile $\rho(z, E)$ ⁴⁸, where z denotes the depth below the surface. Specific experimental details can be found in Refs. 24,33,34, with broader technique overviews provided elsewhere.^{49–51}

In the measurements, it is useful to identify the average field $\langle B \rangle \equiv \int_{-\infty}^{\infty} p(B)B dB$ as a function of E , the latter being proportional to the mean μ^+ stopping depth $\langle z \rangle \equiv \int_0^{\infty} z\rho(z, E) dz$. $\langle B \rangle$ is related to the *true* screening profile $B(z)$ by:

$$\langle B \rangle(E) = \int_0^{\infty} B(z)\rho(z, E) dz, \quad (1)$$

where $\rho(z, E)$ acts as the kernel for the integral transform⁵². In previous work,^{24,33,35} $B(z)$ was found to be consistent with a London model,⁵³ following:

$$B(z) = \tilde{B}_0 \times \begin{cases} 1, & z < d, \\ \exp\left\{-\frac{(z-d)}{\lambda}\right\}, & z \geq d, \end{cases} \quad (2)$$

where λ is the (spatially homogeneous) magnetic penetration depth, d is “dead layer” thickness, and \tilde{B}_0 is the (effective) applied magnetic field:

$$\tilde{B}_0 = B_{\text{applied}} \times \begin{cases} 1, & T \geq T_c, \\ (1 - \tilde{N})^{-1}, & T \ll T_c, \end{cases} \quad (3)$$

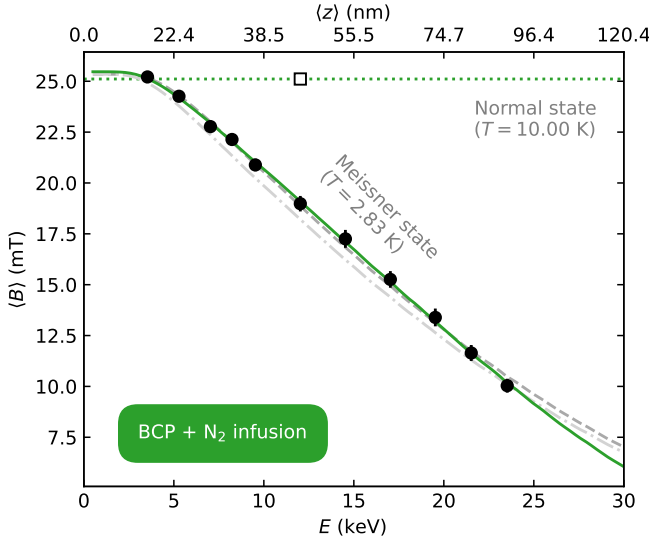


FIG. 3. Meissner screening data in an SRF-grade Nb plate with a “BCP⁴⁶ + N₂ infusion”⁸ surface treatment, obtained from LE- μ SR experiments originally reported in Ref. 33. Here, the mean magnetic field $\langle B \rangle$ is plotted against the muon μ^+ implantation energy E , with its corresponding mean stopping depth $\langle z \rangle$ indicated on a secondary axis. The solid and dotted colored lines denote simultaneous fits of the normal and Meissner state data to Equations (1), (4) and (5). For comparison, the dashed dark gray line shows the form of $\langle B \rangle(E)$ assuming a single (i.e., depth-independent) magnetic penetration depth λ [Equations (1) to (3)]. The dash-dot light gray line denotes this average screening behavior, but with its non-superconducting “dead layer” d adjusted to match the fit using the generalized London equation, highlighting the differences between the two models.

where B_{applied} is the applied magnetic field, $T_c \approx 9.25$ K is Nb’s critical temperature,¹⁹ and \tilde{N} is the sample’s (effective) demagnetization factor (i.e., averaged over the μ^+ beam profile). While this gave a good description of the measurements, the single depth-independent λ in Equation (2) is inconsistent with predictions by others.^{12,15}

To account for spatial inhomogeneities in the Meissner profile, we consider the following generalization of the one-dimension London equation:^{53–56}

$$\lambda^2(z) \left[\frac{d^2 B(z)}{dz^2} \right] + 2\lambda(z) \left[\frac{d\lambda(z)}{dz} \right] \left[\frac{dB(z)}{dz} \right] = B(z), \quad (4)$$

where $B(z)$ is the magnetic field at depth z , and $\lambda(z)$ is the depth-dependent magnetic penetration depth⁵⁷. This expression is often encountered in situations where a spatial dependence to λ is anticipated, such as in proximity-coupled superconductor/normal-metal interfaces (see, e.g., Refs. 54,56). Note that analytic solutions to Equation (4) can only be obtained for select models of $\lambda(z)$,⁵⁶ with the general case requiring numerical methods.⁵⁵ In the context of SRF cavities, it has been proposed that $\lambda(z)$ has the form:¹²

$$\lambda(z) = (\lambda_{\text{surface}} - \lambda_{\text{bulk}}) \operatorname{erfc} \left(\frac{z}{L_D} \right) + \lambda_{\text{bulk}}, \quad (5)$$

where the λ_i s denote the penetration depths at Nb’s surface

and bulk, respectively, with $\lambda(z)$ interpolating the two values over a length scale L_D (e.g., the diffusion length of impurity atoms^{12,15,43}) according to the complimentary error function $\operatorname{erfc}(x) \equiv 1 - (2/\pi) \int_0^x \exp(-y^2) dy$. Alternative approaches for characterizing $\lambda(z)$ have also been proposed, producing qualitatively similar $B(z)$ s.¹⁵

III. RESULTS & DISCUSSION

To quantify the screening behavior explicitly, we fit the LE- μ SR data in Figures 1 to 3, using Equation (1) and numeric solutions to Equation (4), constraining $\lambda(z)$ to follow Equation (5) with $\lambda_{\text{bulk}} = 29$ nm (in accord with “clean” Nb’s literature average^{33,38}), and parameterizing $B(z)$ to contain both a finite d and a geometrically enhanced field $B_{\text{applied}}/(1 - \tilde{N})$, akin to Equations (2) and (3). Fit results are shown in Figures 1 to 3, in good agreement with the measurements. For comparison, screening profiles assuming a spatially homogenous λ [Equations (1) to (3)] are also shown. A summary of these results is given in Table I and we consider the details below.

First, we remark that the results obtained using the two screening models are quite similar; both provide the correct qualitative form of $\langle B \rangle(E)$, yielding virtually identical values for the “experimental” parameters B_{applied} and \tilde{N} (see Table I). Though some quantitative differences are apparent (e.g., the E or $\langle z \rangle$ at which $\langle B \rangle$ begins to decay), both models provide a reasonable description of the Meissner profiles, as evidenced by their goodness-of-fit metric χ_{reduced}^2 . This is expected, given the applicability of the London model in previous work;^{24,33,35} however, we find that the inhomogeneous screening model does a better job of capturing the features of each dataset (see Table I). While this could simply be a result of the fit function’s “extra” degrees-of-freedom (i.e., six vs. four parameters), a judicious inspection of the d values suggest otherwise.

The d s identified by the inhomogeneous screening model are all systematically lower than those extracted assuming a homogeneous Meissner response (see Table I). This is most pronounced for the “EP + 120 °C bake” treatment, with the differences visible by eye in Figure 1. Specifically, the “break in” of $\langle B \rangle$ from the (homogeneous) London model is much more abrupt than the data, in contrast to the smoother curvature of the generalized London equation. In essence, the London model overcompensates for this discrepancy by lengthening d , which we take as evidence for near-surface inhomogeneous screening. Similar behavior is also observed for the “BCP + 120 °C bake” sample (see Figure 2), though the effect is less pronounced. Surprisingly, this “feature” is virtually absent from the “BCP + N₂ infusion” sample, at odds with the results in Ref. 12. It is important to stress that neither treatment^{5,8} meaningfully increases the surface oxide thickness (see, e.g., Ref. 58). At this juncture, we note that the above analysis has only considered the case of local electrodynamics governing Nb’s Meissner response; however, *nonlocal* effects^{59,60} are also known to produce diminished screening close to the surface (see, e.g., Ref. 36). While nonlocal effects are most pronounced in the “clean” limit, they are known to be weak for Nb,³⁶ and on the basis of the impure nature of the sample surfaces (i.e.,

TABLE I. Summary of fit results for the LE- μ SR measurements of the Meissner profiles in SRF Nb samples with LTB surface-treatments. For each sample, its surface-treatment and Meissner profile measurement temperature T is indicated, along values for the fit parameters obtained using Equations (1), (4) and (5) (top three rows) and Equations (1) to (3) (bottom three rows). Here, B_{applied} is the applied magnetic field, \tilde{N} is the (effective) demagnetization factor, d is the non-superconducting “dead layer” thickness, λ is the depth-independent magnetic penetration depth, λ_{surface} is the magnetic penetration depth at the surface, λ_{bulk} is the magnetic penetration depth in the bulk, and L_D is the length scale in Equation (5) over which $\lambda(z)$ changes from λ_{surface} to λ_{bulk} . In each case, the goodness-of-fit metric χ_{reduced}^2 is also provided.

Sample	T (K)	B_{applied} (mT)	\tilde{N}	d (nm)	λ (nm)	λ_{surface} (nm)	λ_{bulk} (nm)	L_D (nm)	χ_{reduced}^2
EP + 120 °C bake	3.00	9.58(4) / 24.33(6)	0.069(11) / 0.017(11)	26(4)		78(12)	29	63(9)	0.91
BCP + 120 °C bake	2.72	25.179(34)	0.014(10)	20.9(22)		54(6)	29	57(12)	1.75
BCP + N ₂ infusion	2.83	25.11(6)	0.014(10)	21.3(23)		75(5)	29	140(60)	0.44
EP + 120 °C bake	3.00	9.58(4) / 24.33(6)	0.059(9) / 0.007(9)	34.9(14)	52.5(18)				1.73
BCP + 120 °C bake	2.72	25.179(34)	0.006(11)	25.4(13)	42.6(13)				2.09
BCP + N ₂ infusion	2.83	25.11(6)	0.009(11)	24.1(17)	70.2(26)				0.62

from their LTB treatments),^{8,13,15} we rule out their importance. Thus, we take the differences in the d s identified by each model, in conjunction with the overall fit quality χ_{reduced}^2 , as evidence supporting inhomogeneous near-surface field screening⁶¹.

Further evidence supporting this notion can be gleaned from the remaining fit parameters. For the two “120 °C bake”⁵ samples, despite their different surface polishings (i.e., EP vs. BCP),⁴⁶ we find that their λ_{surface} and L_D values are similar, suggesting the observed screening behavior is intrinsic for the treatment. Taking their weighted average, we find $L_D = 61(7)$ nm, which is comparable to the spatial extent of the oxygen impurity profile induced by baking,^{10,13,15} and $\lambda_{\text{surface}} = 59(5)$ nm, consistent with “dirty” Nb (cf. $\lambda \approx 29$ nm for “clean” Nb^{33,38}). Importantly, for both samples we find that $\lambda_{\text{surface}} > \lambda$, implying that the screening capacity near the surface is weaker than the average over the first ~ 150 nm.³³ Together, we take this consistency as further support of inhomogeneous screening caused by LTB in vacuum.

In contrast, the evidence for inhomogeneous Meissner screening in the N₂ infusion sample is less compelling. Contrary to expectations from surface etching¹² and secondary ion mass spectrometry (SIMS)⁸ measurements, our identified L_D is large compared to the extent of near-surface nitrogen defects and its sizeable uncertainty hinders drawing firm conclusions about this length scale. Similarly, λ_{surface} was found to be close to the homogeneous λ value, implying that inhomogeneities in the Meissner response are either: 1) absent from this treatment; 2) beyond the resolution of the LE- μ SR measurements; or 3) transpiring over depths greater than those probed in the experiments. Note that the close agreement between screening models is mirrored by their $\chi_{\text{reduced}}^2 < 1$, implying that the data is overparameterized (even in the simplest case). Thus, we conclude that the current data do not support the notion of inhomogeneous screening caused by N₂ infusion; however, further experiments are required to be more conclusive.⁶²

To further test the above findings on LTB, we also considered an additional refinement to the Meissner profile analyses shown in Figures 2 and 3. Noting that these data³³ originate from a common batch of samples where an independent control is available (i.e., a sample with only a “BCP” treatment — called “baseline” in Ref. 33), we re-fit the LTB data *simultaneously* using Equations (1), (4) and (5), but used the “BCP” sample’s screening profile to constrain λ_{bulk} (i.e., using Equations (1)

to (3)). As both the sample dimensions and measurement conditions are common to these Nb plates,³³ under the assumption that their “true” d is also identical, we additionally restricted the simultaneous fit so that B_{applied} , \tilde{N} , and d were treated as shared parameters. The culmination of this exercise is shown in Figure 4, with values for the optimum parameters displayed in its inset. Clearly, these restrictions pose no impediment to the form of the inhomogeneous screening in the LTB samples, as reflected by the good agreement of their λ_{surface} and L_D values with those in Table I. Moreover, the fit’s common parameters (see Figure 4’s top panel) are in excellent agreement with the values reported previously for the “BCP” sample,³³ indicating that the fitting procedure has no adverse effect on describing its screening behavior. This is further confirmed by their consistency with the tabulation in Table I, apart from λ_{bulk} ’s ~ 2.6 nm difference. This difference, albeit small, suggests that the inhomogeneous screening model is not strongly sensitive to λ_{bulk} ’s absolute value, making the literature average (29 nm)^{33,38} used when fitting the data in Figures 1 to 3 a reasonable choice. Overall, these results show that having an independent means of characterizing the “bulk” screening properties can greatly reduce the uncertainty in quantifying the inhomogeneous portion of the Meissner profile.

As a final remark, we note that neither of the original LE- μ SR measurements^{24,33} were optimized for the detection of Meissner profile inhomogeneities, instead focusing on their overall (i.e., average) form. In future measurements, it is apparent from Figures 1 to 3 that two regions are important to focus on: 1) the near-surface region (i.e., $z \lesssim 40$ nm), where the gradual curvature of $B(z)$ is most pronounced; and 2) deep below the surface (i.e., $z \gtrsim 120$ nm), where the decay of $B(z)$ becomes close to its “bulk” behavior. While the former was suggested previously,³⁵ the latter is only evident upon inspection of the fit curves when extrapolated beyond the current data. Having $\langle B \rangle$ measurements in this region ($E \gtrsim 25$ keV) is likely crucial for independently identifying λ_{bulk} (i.e., in the absence of a separate “control” sample), as well as reducing the (rather large) uncertainty in the inhomogeneous screening model’s fit parameters. Similarly, it would be beneficial to characterize the impurity content in the studied samples directly, (e.g., using SIMS^{63,64}), and parameterize $\lambda(z)$ directly (i.e., from their influence on the electron mean-free-path ℓ ^{21,22} — see Ref. 15).

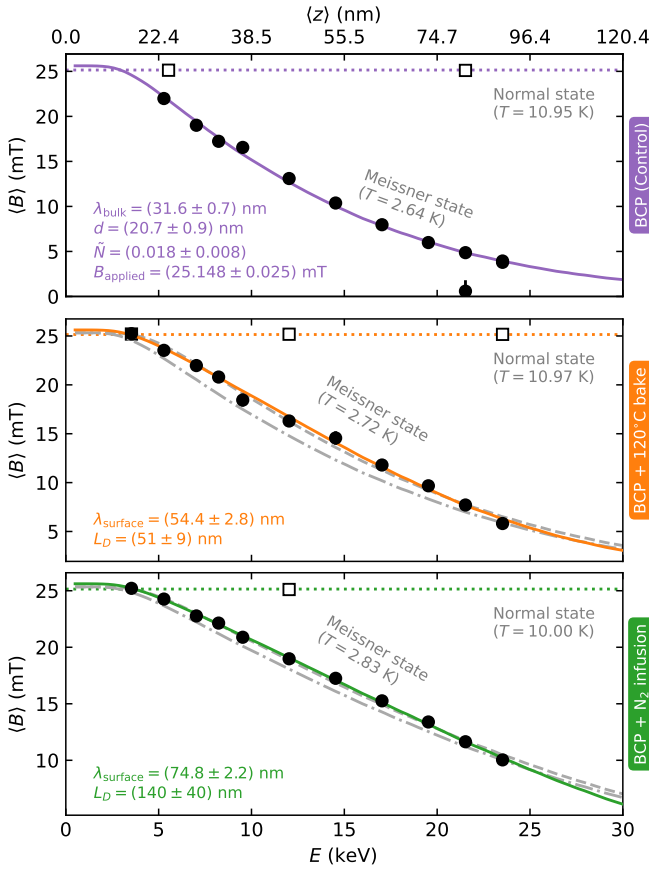


FIG. 4. Meissner screening data in a SRF-grade Nb plates with “BCP⁴⁶” (top panel), “BCP⁴⁶ + 120 °C bake⁵” (middle panel), and “BCP⁴⁶ + N₂ infusion⁸” (bottom panel) surface treatments, obtained from LE- μ SR experiments originally reported in Ref. 33. Here, the mean magnetic field $\langle B \rangle$ is plotted against the muon μ^+ implantation energy E , with its corresponding mean stopping depth $\langle z \rangle$ indicated on a secondary axis. The solid and dotted colored lines denote simultaneous fits of the normal and Meissner state data in *all* samples, using Equations (1) to (3) for the “BCP” treatment (i.e., as a control) and Equations (1), (4) and (5) for the LTB samples, with the optimum parameters listed in the panel insets. For comparison, in the middle and bottom panels the dashed dark gray line shows the form of $\langle B \rangle(E)$ assuming a single (i.e., depth-independent) magnetic penetration depth λ [Equations (1) to (3)] in the LTB sample. Similarly, the dash-dot light gray line denotes this average screening behavior, but with its non-superconducting “dead layer” d adjusted to match the fit using the generalized London equation, highlighting the differences between the two models.

IV. SUMMARY

In summary, we revisited the Meissner profile data for Nb samples^{24,33,35} with surfaces prepared using LTB treatments^{5,8} common to SRF cavities. By comparing results obtained from fits to a (homogeneous) London equation⁵³ and the generalized London expression^{53–56} with an empirical model for a depth-dependent magnetic penetration depth $\lambda(z)$,¹² we identify the presence of a large non-superconducting “dead layer” $d \gtrsim 25$ nm as a likely indicator for inhomogeneities in the

near-surface Meissner response. The inhomogeneities are most apparent for the “120 °C bake” treatment,⁵ with the extracted length scale between “surface” and “bulk” behavior in good agreement with both experiment¹⁰ theory.^{13,15} Conversely, they are essentially absent for the “N₂ infusion” treatment,⁸ in contrast to another report.¹² Further LE- μ SR measurements, covering both shallow ($z \lesssim 40$ nm) and deep ($z \gtrsim 120$ nm) subsurface depths, will aid in precisely quantifying this phenomenon.

ACKNOWLEDGMENTS

We thank M. Asaduzzaman and E. M. Lechner for useful discussions and a critical reading of the manuscript. T. Junginger acknowledges financial support from NSERC.

AUTHOR DECLARATIONS

Conflict of Interest

The authors have no conflicts to disclose.

Author Contributions

Ryan M. L. McFadden: Conceptualization (lead); Data Curation (lead); Formal Analysis (lead); Software (lead); Visualization (lead); Writing — Original Draft Preparation (lead); Writing — Review and Editing (lead). **Tobias Junginger:** Conceptualization (supporting); Funding Acquisition (lead); Writing — Review and Editing (supporting).

DATA AVAILABILITY

Raw data from the LE- μ SR measurements reported in Refs. 24,33 were generated at the Swiss Muon Source (S μ S), Paul Scherrer Institute (PSI), Villigen, Switzerland. Individual data files and derived data supporting the findings of this work are available from the corresponding authors upon reasonable request.

¹H. Padamsee, J. Knobloch, and T. Hays, *RF Superconductivity for Accelerators*, 2nd ed., Wiley Series in Beam Physics and Accelerator Technology (Wiley, New York, 2008).

²H. Padamsee, *RF Superconductivity: Science, Technology, and Applications* (Wiley, Weinheim, 2009).

³H. Padamsee, *Superconducting Radiofrequency Technology for Accelerators: State of the Art and Emerging Trends* (Wiley, Weinheim, 2023).

⁴A. Gurevich, “Tuning microwave losses in superconducting resonators,” *Supercond. Sci. Technol.* **36**, 063002 (2023).

⁵G. Ciovati, “Effect of low-temperature baking on the radio-frequency properties of niobium superconducting cavities for particle accelerators,” *J. Appl. Phys.* **96**, 1591–1600 (2004).

⁶A. Grassellino, A. Romanenko, D. Bice, O. Melnychuk, A. C. Crawford, S. Chandrasekaran, Z. Sung, D. A. Sergatskov, M. Checchin, S. Posen, M. Martinello, and G. Wu, “Accelerating fields up to 49 MV m⁻¹ in TESLA-shape superconducting RF niobium cavities via 75 °C vacuum bake,” [arXiv:1806.09824](https://arxiv.org/abs/1806.09824) [physics.acc-ph].

- ⁷A. Grassellino, A. Romanenko, D. Sergatskov, O. Melnychuk, Y. Trenikhina, A. Crawford, A. Rowe, M. Wong, T. Khabiboulline, and F. Barkov, "Nitrogen and argon doping of niobium for superconducting radio frequency cavities: a pathway to highly efficient accelerating structures," *Supercond. Sci. Technol.* **26**, 102001 (2013).
- ⁸A. Grassellino, A. Romanenko, Y. Trenikhina, M. Checchin, M. Martinello, O. S. Melnychuk, S. Chandrasekaran, D. A. Sergatskov, S. Posen, A. C. Crawford, S. Aderhold, and D. Bice, "Unprecedented quality factors at accelerating gradients up to 45 MV m⁻¹ in niobium superconducting resonators via low temperature nitrogen infusion," *Supercond. Sci. Technol.* **30**, 094004 (2017).
- ⁹L. Lilje, D. Reschke, K. Twarowski, P. Schmüser, D. Bloess, E. Chiaveri, E. Haebel, H. Preis, J.-M. Tessier, H. Wenninger, J. P. Charrier, and H. Safa, "Electropolishing and in-situ baking of 1.3 GHz niobium cavities," in *Proceedings of SRF1999*, Workshop on RF Superconductivity No. 9, Los Alamos National Laboratory (JACoW Publishing, Geneva, Switzerland, 1999) pp. 74–76.
- ¹⁰A. Romanenko, A. Grassellino, F. Barkov, and J. P. Ozelis, "Effect of mild baking on superconducting niobium cavities investigated by sequential nanoremoval," *Phys. Rev. ST Accel. Beams* **16**, 012001 (2013).
- ¹¹P. Dhakal, S. Chetri, S. Balachandran, P. J. Lee, and G. Ciovati, "Effect of low temperature baking in nitrogen on the performance of a niobium superconducting radio frequency cavity," *Phys. Rev. Accel. Beams* **21**, 032001 (2018).
- ¹²M. Checchin and A. Grassellino, "High-field Q-slope mitigation due to impurity profile in superconducting radio-frequency cavities," *Appl. Phys. Lett.* **117**, 032601 (2020).
- ¹³G. Ciovati, "Improved oxygen diffusion model to explain the effect of low-temperature baking on high field losses in niobium superconducting cavities," *Appl. Phys. Lett.* **89**, 022507 (2006).
- ¹⁴T. Kubo and A. Gurevich, "Field-dependent nonlinear surface resistance and its optimization by surface nanostructuring in superconductors," *Phys. Rev. B* **100**, 064522 (2019).
- ¹⁵E. M. Lechner, J. W. Angle, A. D. Palczewski, F. A. Stevie, M. J. Kelley, and C. E. Reece, "Oxide dissolution and oxygen diffusion scenarios in niobium and implications on the Bean-Livingston barrier in superconducting cavities," *J. Appl. Phys.* **135**, 133902 (2024).
- ¹⁶T. Junginger, W. Wasserman, and R. E. Laxdal, "Superheating in coated niobium," *Supercond. Sci. Technol.* **30**, 125012 (2017).
- ¹⁷T. Junginger, S. H. Abidi, R. D. Maffett, T. Buck, M. H. Dehn, S. Gheidi, R. Kiefl, P. Kolb, D. Storey, E. Thoeng, W. Wasserman, and R. E. Laxdal, "Field of first magnetic flux entry and pinning strength of superconductors for rf application measured with muon spin rotation," *Phys. Rev. Accel. Beams* **21**, 032002 (2018).
- ¹⁸T. Kubo, "Superheating fields of semi-infinite superconductors and layered superconductors in the diffusive limit: structural optimization based on the microscopic theory," *Supercond. Sci. Technol.* **34**, 045006 (2021).
- ¹⁹D. A. Turner, G. Burt, and T. Junginger, "No interface energy barrier and increased surface pinning in low temperature baked niobium," *Sci. Rep.* **12**, 5522 (2022).
- ²⁰M. Asaduzzaman, R. M. L. McFadden, E. Thoeng, R. E. Laxdal, and T. Junginger, "Measurements of the first-flux-penetration field in surface-treated and coated Nb: distinguishing between near-surface pinning and an interface energy barrier," *Supercond. Sci. Technol.* **37**, 085006 (2024).
- ²¹B. B. Goodman and G. Kuhn, "Influence des défauts étendus sur les propriétés supraconductrices du niobium," *J. Phys. France* **29**, 240–252 (1968).
- ²²K. Schulze, J. Fuß, H. Schultz, and S. Hofmann, "Einfluß interstitieller fremdatome auf den restwiderstand von reinem niob," *Z. Metallkd.* **67**, 737–743 (1976).
- ²³V. Ngampruetikorn and J. A. Sauls, "Effect of inhomogeneous surface disorder on the superheating field of superconducting RF cavities," *Phys. Rev. Res.* **1**, 012015(R) (2019).
- ²⁴A. Romanenko, A. Grassellino, F. Barkov, A. Suter, Z. Salman, and T. Prokscha, "Strong Meissner screening change in superconducting radio frequency cavities due to mild baking," *Appl. Phys. Lett.* **104**, 072601 (2014).
- ²⁵M. Checchin, *Physics of Limiting Phenomena in Superconducting Microwave Resonators: Vortex Dissipation, Ultimate Quench and Quality Factor Degradation Mechanisms*, Ph.D. thesis, Illinois Institute of Technology, Chicago, IL (2016).
- ²⁶M. Checchin, A. Grassellino, M. Martinello, S. Posen, A. Romanenko, and J. Zasadzinski, "Ultimate gradient limitation in niobium superconducting accelerating cavities," in *Proceedings of IPAC'16*, International Particle Accelerator Conference No. 7 (JACoW Publishing, Geneva, Switzerland, 2016) pp. 2254–2257.
- ²⁷T. Kubo, "Multilayer coating for higher accelerating fields in superconducting radio-frequency cavities: a review of theoretical aspects," *Supercond. Sci. Technol.* **30**, 023001 (2017).
- ²⁸A. Gurevich, "Enhancement of rf breakdown field of superconductors by multilayer coating," *Appl. Phys. Lett.* **88**, 012511 (2006).
- ²⁹T. Kubo, Y. Iwashita, and T. Saeki, "Radio-frequency electromagnetic field and vortex penetration in multilayered superconductors," *Appl. Phys. Lett.* **104**, 032603 (2014).
- ³⁰A. Gurevich, "Maximum screening fields of superconducting multilayer structures," *AIP Adv.* **5**, 017112 (2015).
- ³¹S. Posen, M. K. Transtrum, G. Catelani, M. U. Liepe, and J. P. Sethna, "Shielding superconductors with thin films as applied to rf cavities for particle accelerators," *Phys. Rev. Appl.* **4**, 044019 (2015).
- ³²This finding in Ref. 27 is noteworthy, as it demonstrates how inhomogeneous screening properties lead to the suppression of surface supercurrents, which in turn increase Nb's superheating field B_{sh} (i.e., the maximum magnetic field to which the metal can remain in a (metastable) flux-free state) — an operational limit realized by state-of-the-art SRF cavities (see, e.g., Refs. 3, 4).
- ³³R. M. L. McFadden, M. Asaduzzaman, T. Prokscha, Z. Salman, A. Suter, and T. Junginger, "Depth-resolved measurements of the Meissner screening profile in surface-treated Nb," *Phys. Rev. Appl.* **19**, 044018 (2023).
- ³⁴M. Asaduzzaman, R. M. L. McFadden, A.-M. Valente-Feliciano, D. R. Beverstock, A. Suter, Z. Salman, T. Prokscha, and T. Junginger, "Evidence for current suppression in superconductor-superconductor bilayers," *Supercond. Sci. Technol.* **37**, 025002 (2024).
- ³⁵R. M. L. McFadden, M. Asaduzzaman, and T. Junginger, "Comment on "Strong Meissner screening change in superconducting radio frequency cavities due to mild baking" [Appl. Phys. Lett. 104, 072601 (2014)]," *Appl. Phys. Lett.* **124**, 086101 (2024).
- ³⁶A. Suter, E. Morenzoni, N. Garifanov, R. Khasanov, E. Kirk, H. Luetkens, T. Prokscha, and M. Horisberger, "Observation of nonexponential magnetic penetration profiles in the Meissner state: A manifestation of nonlocal effects in superconductors," *Phys. Rev. B* **72**, 024506 (2005).
- ³⁷T. Junginger, S. Calatroni, A. Sublet, G. Terenziani, T. Prokscha, Z. Salman, A. Suter, T. Proslir, and J. Zasadzinski, "A low energy muon spin rotation and point contact tunneling study of niobium films prepared for superconducting cavities," *Supercond. Sci. Technol.* **30**, 125013 (2017).
- ³⁸R. M. L. McFadden, M. Asaduzzaman, T. J. Buck, D. L. Cortie, M. H. Dehn, S. R. Dunsiger, R. F. Kiefl, R. E. Laxdal, C. D. P. Levy, W. A. MacFarlane, G. D. Morris, M. R. Pearson, E. Thoeng, and T. Junginger, "Depth-resolved measurement of the Meissner screening profile in a niobium thin film from spin-lattice relaxation of the implanted β -emitter ^8Li ," *J. Appl. Phys.* **134**, 163902 (2023).
- ³⁹M. Lindstrom, B. Wetton, and R. Kiefl, "Mathematical modelling of the effect of surface roughness on magnetic field profiles in type II superconductors," *J. Eng. Math.* **85**, 149–177 (2014).
- ⁴⁰M. Lindstrom, A. C. Y. Fang, and R. F. Kiefl, "Effect of surface roughness on the magnetic field profile in the Meissner state of a superconductor," *J. Supercond. Novel Magn.* **29**, 1499–1507 (2016).
- ⁴¹J. Halbritter, "On the oxidation and on the superconductivity of niobium," *Appl. Phys. A* **43**, 1–28 (1987).
- ⁴²A. Romanenko, Y. Trenikhina, M. Martinello, D. Bafia, and A. Grassellino, "First direct imaging and profiling TOF-SIMS studies on cutouts from cavities prepared by state-of-the-art treatments," in *Proceedings of SRF'19*, International Conference on RF Superconductivity No. 19, Helmholtz Zentrum Dresden (JACoW Publishing, Geneva, Switzerland, 2019) pp. 866–870.
- ⁴³E. M. Lechner, J. W. Angle, F. A. Stevie, M. J. Kelley, C. E. Reece, and A. D. Palczewski, "RF surface resistance tuning of superconducting niobium via thermal diffusion of native oxide," *Appl. Phys. Lett.* **119**, 082601 (2021).
- ⁴⁴P. Bakule and E. Morenzoni, "Generation and applications of slow polarized muons," *Contemp. Phys.* **45**, 203–225 (2004).
- ⁴⁵E. Morenzoni, T. Prokscha, A. Suter, H. Luetkens, and R. Khasanov, "Nano-scale thin film investigations with slow polarized muons," *J. Phys.: Condens. Matter* **16**, S4583–S4601 (2004).

- ⁴⁶G. Ciovati, H. Tian, and S. G. Corcoran, “Buffered electrochemical polishing of niobium,” *J. Appl. Electrochem.* **41**, 721–730 (2011).
- ⁴⁷E. Morenzoni, H. Glückler, T. Prokscha, R. Khasanov, H. Luetkens, M. Birke, E. M. Forgan, C. Niedermayer, and M. Pleines, “Implantation studies of keV positive muons in thin metallic layers,” *Nucl. Instrum. Methods Phys. Res., Sect. B* **192**, 254–266 (2002).
- ⁴⁸For typical μ^+ stopping profiles in Nb at $E \leq 30$ keV, see Fig. 1 in Ref. 33.
- ⁴⁹S. J. Blundell, R. De Renzi, T. Lancaster, and F. L. Pratt, eds., *Muon Spectroscopy: An Introduction* (Oxford University Press, Oxford, 2021).
- ⁵⁰A. D. Hillier, S. J. Blundell, I. McKenzie, I. Umegaki, L. Shu, J. A. Wright, T. Prokscha, F. Bert, K. Shimomura, A. Berlie, H. Alberto, and I. Watanabe, “Muon spin spectroscopy,” *Nat. Rev. Methods Primers* **2**, 4 (2022).
- ⁵¹A. Amato and E. Morenzoni, *Introduction to Muon Spin Spectroscopy: Applications to Solid State and Material Sciences*, Lecture Notes in Physics, Vol. 961 (Springer Nature Switzerland AG, Cham, 2024).
- ⁵²Note that $\rho(z, E)$ is not directly determined by the measurement; however, it can be accurately quantified using Monte Carlo simulations for μ^+ implantation.^{33,47} While the simulation results are generally obtained at discrete E , they can be made continuous using empirical “interpolation” schemes,^{33,34} facilitating the evaluation of Equation (1).
- ⁵³F. London and H. London, “The electromagnetic equations of the supraconductor,” *Proc. R. Soc. London A* **149**, 71–88 (1935).
- ⁵⁴R. W. Simon and P. M. Chaikin, “Josephson tunneling studies of magnetic screening in proximity-superconducting silver,” *Phys. Rev. B* **23**, 4463–4469 (1981).
- ⁵⁵J. R. Cave and J. E. Evetts, “Critical temperature profile determination using a modified London equation for inhomogeneous superconductors,” *J. Low Temp. Phys.* **63**, 35–55 (1986).
- ⁵⁶M. S. Pambianchi, J. Mao, and S. M. Anlage, “Magnetic screening in proximity-coupled superconductor/normal-metal bilayers,” *Phys. Rev. B* **50**, 13659–13663 (1994).
- ⁵⁷Note that when $d\lambda(z)/dz = 0$ (i.e., when $\lambda(z)$ is depth-independent), Equation (4) reduces to the familiar London expression,⁵³ whose solution $B(z) \propto \exp(-z/\lambda)$ is akin to Equation (2).
- ⁵⁸A. Prudnikava, Y. Tamashevich, S. Babenkov, A. Makarova, D. Smirnov, V. Aristov, O. Molodtsova, O. Kugeler, J. Viehhaus, and B. Foster, “Systematic study of niobium thermal treatments for superconducting radio frequency cavities employing x-ray photoelectron spectroscopy,” *Supercond. Sci. Technol.* **35**, 065019 (2022).
- ⁵⁹A. B. Pippard, “An experimental and theoretical study of the relation between magnetic field and current in a superconductor,” *Proc. R. Soc. London A* **216**, 547–568 (1953).
- ⁶⁰J. Bardeen, L. N. Cooper, and J. R. Schrieffer, “Theory of superconductivity,” *Phys. Rev.* **108**, 1175–1204 (1957).
- ⁶¹As a check of this conclusion, we also compared fits of the homogeneous and inhomogeneous screening models to “clean” Nb with a BCP surface (i.e., the “baseline” sample in Ref. 33), finding no meaningful differences.
- ⁶²We note that there are reproducibility challenges associated with the N₂ infusion “recipe,”⁸ with precise control over the treatment conditions (e.g., cavity temperature, vacuum quality, furnace cleanliness, etc.) likely being crucial.^{11,58} In the future, having samples treated *in situ* with SRF cavities that explicitly show HFQS amelioration would be beneficial.
- ⁶³J. W. Angle, A. D. Palczewski, C. E. Reece, F. A. Stevie, and M. J. Kelley, “Advances in secondary ion mass spectrometry for N-doped niobium,” *J. Vac. Sci. Technol. B* **39**, 024004 (2021).
- ⁶⁴J. W. Angle, E. M. Lechner, A. D. Palczewski, C. E. Reece, F. A. Stevie, and M. J. Kelley, “Improved quantitation of SIMS depth profile measurements of niobium via sample holder design improvements and characterization of grain orientation effects,” *J. Vac. Sci. Technol. B* **40**, 024003 (2022).